EUROPEAN ORGANIZATION FOR NUCLEAR RESEARCH

CERN–PPE/95-28

14 March 1995

Inclusive Measurements of the $K^{\pm}$ and $p/\overline{p}$ Production in Hadronic Z^0 Decays

DELPHI Collaboration

Abstract

This analysis, based on a sample of 170,000 hadronic Z^0 decays, provides a measurement of the $K^{\pm}$ and $p/\overline{p}$ differential cross-sections which is compared to string- and cluster fragmentation models. The total multiplicities for $K^{\pm}$ and $p/\overline{p}$ per hadronic event were found to be: $N_K = 2.26 \pm 0.18$ and $N_p = 1.07 \pm 0.14$. The positions ξ^* of the maxima of the differential cross-sections as a function of $\xi = \ln(1/x_p)$ for $K^{\pm}$ and $p/\overline{p}$ were determined to be 2.63 ± 0.07 and 2.96 ± 0.16 respectively. A comparison of the ξ^* values for various identified particles measured at LEP with the prediction of the Modified Leading Logarithm Approximation with Local Parton Hadron Duality model has been performed. The measured ξ^* position as a function of the hadron mass, after corrections due to particle decays, is in agreement with the model calculation.

(To be submitted to Nuclear Physics B)

P.Abreu[21], W.Adam[50], T.Adye[37], E.Agasi[31], I.Ajinenko[42], R.Aleksan[39], G.D.Alekseev[16], P.P.Allport[22], S.Almehed[24], S.J.Alvsvaag[4], U.Amaldi[9], S.Amato[47], A.Andreazza[28], M.L.Andrieux[14], P.Antilogus[25], W-D.Apel[17], Y.Arnoud[39], B.Åsman[44], J-E.Augustin[19], A.Augustinus[31], P.Baillon[9], P.Bambade[19], F.Barao[21], R.Barate[14], D.Y.Bardin[16], G.J.Barker[35], A.Baroncelli[40], O.Barring[24], J.A.Barrio[26], W.Bartl[50], M.J.Bates[37], M.Battaglia[15], M.Baubillier[23], J.Baudot[39], K-H.Becks[52], M.Begalli[6], P.Beilliere[8], Yu.Belokopytov[9], K.Belous[42], A.C.Benvenuti[5], M.Berggren[41], D.Bertrand[2], F.Bianchi[45], M.Bigi[45], M.S.Bilenky[16], P.Billoir[23], J.Bjarne[24], D.Bloch[10], M.Blume[52], S.Blyth[35], V.Bocci[38], T.Bolognese[39], M.Bonesini[28], W.Bonivento[28], P.S.L.Booth[22], G.Borisov[42], C.Bosio[40], B.Bostjancic[43], S.Bosworth[35], O.Botner[48], E.Boudinov[42], B.Bouquet[19], C.Bourdarios[9], T.J.V.Bowcock[22], M.Bozzo[13], P.Branchini[40], K.D.Brand[36], R.A.Brenner[15], C.Bricman[2], L.Brillault[23], R.C.A.Brown[9], P.Bruckman[18], J-M.Brunet[8], L.Bugge[33], T.Buran[33], A.Buys[9], M.Caccia[28], M.Calvi[28], A.J.Camacho Rozas[41], T.Camporesi[9], V.Canale[38], M.Canepa[13], K.Cankocak[44], F.Cao[2], F.Carena[9], P.Carrilho[47], L.Carroll[22], C.Caso[13], V.Cassio[45], M.V.Castillo Gimenez[49], A.Cattai[9], F.R.Cavallo[5], L.Cerrito[38], V.Chabaud[9], Ph.Charpentier[9], L.Chaussard[25], J.Chauveau[23], P.Checchia[36], G.A.Chelkov[16], P.Chliapnikov[42], P.Chochula[7], V.Chorowicz[9], V.Cindro[43], P.Collins[9], J.L.Contreras[19], R.Contri[13], E.Cortina[49], G.Cosme[19], F.Cossutti[46], H.B.Crawley[1], D.Crennell[37], G.Crosetti[13], J.Cuevas Maestro[34], S.Czellar[15], E.Dahl-Jensen[29], J.Dahm[52], B.Dalmagne[19], M.Dam[33], G.Damgaard[29], A.Daum[17], P.D.Dauncey[37], M.Davenport[9], W.Da Silva[23], C.Defoix[8], G.Della Ricca[46], P.Delpierre[27], N.Demaria[35], A.De Angelis[9], H.De Boeck[2], W.De Boer[17], S.De Brabandere[2], C.De Clercq[2], C.De La Vaissiere[23], B.De Lotto[46], A.De Min[28], L.De Paula[47], C.De Saint-Jean[39], H.Dijkstra[9], L.Di Ciaccio[38], F.Djama[10], J.Dolbeau[8], M.Donszelmann[9], K.Doroba[51], M.Dracos[10], J.Drees[52], K.-A.Drees[52], M.Dris[32], Y.Dufour[8], F.Dupont[14], D.Edsall[1], R.Ehret[17], G.Eigen[4], T.Ekelof[48], G.Ekspong[44], M.Elsing[52], J-P.Engel[10], N.Ershaidat[23], M.Espirito Santo[21], V.Falaleev[42], D.Fassouliotis[32], M.Feindt[9], A.Ferrer[49], T.A.Filippas[32], A.Firestone[1], H.Foeth[9], E.Fokitis[32], F.Fontanelli[13], F.Formenti[9], B.Franek[37], P.Frenkiel[8], D.C.Fries[17], A.G.Frodesen[4], R.Fruhwirth[50], F.Fulda-Quenzer[19], H.Furstenau[9], J.Fuster[49], D.Gamba[45], M.Gandelman[6], C.Garcia[49], J.Garcia[41], C.Gaspar[9], U.Gasparini[36], Ph.Gavillet[9], E.N.Gazis[32], D.Gele[10], J-P.Gerber[10], D.Gillespie[9], R.Gokieli[51], B.Golob[43], G.Gopal[37], L.Gorn[1], M.Gorski[51], V.Gracco[13], F.Grard[2], E.Graziani[40], G.Grosdidier[19], P.Gunnarsson[44], M.Gunther[48], J.Guy[37], U.Haedinger[17], F.Hahn[52], M.Hahn[17], S.Hahn[52], S.Haider[31], Z.Hajduk[18], A.Hakansson[24], A.Hallgren[48], K.Hamacher[52], W.Hao[31], F.J.Harris[35], V.Hedberg[24], R.Henriques[21], J.J.Hernandez[49], P.Herquet[2], H.Herr[9], T.L.Hessing[9], E.Higon[49], H.J.Hilke[9], T.S.Hill[1], S-O.Holmgren[44], P.J.Holt[35], D.Holthuizen[31], M.Houlden[22], J.Hrubec[50], K.Huet[2], K.Hultqvist[44], P.Ioannou[3], J.N.Jackson[22], R.Jacobsson[44], P.Jalocha[18], R.Janik[7], G.Jarlskog[24], P.Jarry[39], B.Jean-Marie[19], E.K.Johansson[44], L.Jonsson[24], C.Joram[9], P.Juillot[10], M.Kaiser[17], G.Kalmus[37], F.Kapusta[23], M.Karlsson[44], E.Karvelas[11], S.Katsanevas[3], E.C.Katsoufis[32], R.Keranen[15], B.A.Khomenko[16], N.N.Khovanski[16], B.King[22], N.J.Kjaer[29], H.Klein[9], A.Klovning[4], P.Kluit[31], J.H.Koehne[17], B.Koene[31], P.Kokkinias[11], M.Koratzinos[9], V.Kostioukhine[42], C.Kourkoumelis[3], O.Kouznetsov[13], P.-H.Kramer[52], C.Kreuter[17], J.Krolikowski[51], I.Kronkvist[24], Z.Krumstein[16], W.Krupinski[18], P.Kubinec[7], W.Kucewicz[18], K.Kurvinen[15], C.Lacasta[49], I.Laktineh[25], S.Lamblot[23], J.W.Lamsa[1], L.Lanceri[46], D.W.Lane[1], P.Langefeld[52], V.Lapin[42], I.Last[22], J-P.Laugier[39], R.Lauhakangas[15], G.Leder[50], F.Ledroit[14], V.Lefebure[2], C.K.Legan[1], R.Leitner[30], Y.Lemoigne[39], J.Lemonne[2], G.Lenzen[52], V.Lepeltier[19], T.Lesiak[36], D.Liko[50], R.Lindner[52], A.Lipniacka[19], I.Lippi[36], B.Loerstad[24], M.Lokajicek[12], J.G.Loken[35], J.M.Lopez[41], A.Lopez-Fernandez[9], M.A.Lopez Aguera[41], D.Loukas[11], P.Lutz[39], L.Lyons[35], J.MacNaughton[50], G.Maehlum[17], A.Maio[21], V.Malychev[16], F.Mandl[50], J.Marco[41], B.Marechal[47], M.Margoni[36], J-C.Marin[9], C.Mariotti[40], A.Markou[11], T.Maron[52], C.Martinez-Rivero[41], F.Martinez-Vidal[49], S.Marti i Garcia[49], F.Matorras[41], C.Matteuzzi[28], G.Matthiae[38], M.Mazzucato[36], M.Mc Cubbin[9], R.Mc Kay[1], R.Mc Nulty[22], J.Medbo[48], C.Meroni[28], W.T.Meyer[1], M.Michelotto[36], E.Migliore[45], L.Mirabito[25], W.A.Mitaroff[50], U.Mjoernmark[24], T.Moa[44], R.Moeller[29], K.Moenig[9], M.R.Monge[13], P.Morettini[13], H.Mueller[17], L.M.Mundim[6], W.J.Murray[37], B.Muryn[18], G.Myatt[35], F.Naraghi[14], F.L.Navarria[5], S.Navas[49], P.Negri[28], S.Nemecek[12], W.Neumann[52], N.Neumeister[50], R.Nicolaidou[3], B.S.Nielsen[29], V.Nikolaenko[25], P.Niss[44], A.Nomerotski[36], A.Normand[35], W.Oberschulte-Beckmann[17], V.Obraztsov[42], A.G.Olshevski[16], A.Onofre[21], R.Orava[15], K.Osterberg[15], A.Ouraou[39], P.Paganini[19], M.Paganoni[28], P.Pages[10], H.Palka[18], Th.D.Papadopoulou[32], L.Pape[9], F.Parodi[13], A.Passeri[40], M.Pegoraro[36], J.Pennanen[15], H.Pernegger[50], M.Pernicka[50], A.Perrotta[5], C.Petridou[46], A.Petrolini[13], H.T.Phillips[37], G.Piana[13], F.Pierre[39], M.Pimenta[21], S.Plaszczynski[19], O.Podobrin[17], M.E.Pol[6], G.Polok[18], P.Poropat[46], V.Pozdniakov[16], M.Prest[46], P.Privitera[38], A.Pullia[28], D.Radojicic[35], S.Ragazzi[28], H.Rahmani[32], J.Rames[12], P.N.Ratoff[20], A.L.Read[33], M.Reale[52], P.Rebecchi[19], N.G.Redaelli[28], M.Regler[50], D.Reid[9], P.B.Renton[35], L.K.Resvanis[3], F.Richard[19], J.Richardson[22], J.Ridky[12], G.Rinaudo[45], I.Ripp[39], A.Romero[45], I.Roncagliolo[13], P.Ronchese[36], L.Roos[14], E.I.Rosenberg[1], E.Rosso[9], P.Roudeau[19], T.Rovelli[5], W.Ruckstuhl[31], V.Ruhlmann-Kleider[39], A.Ruiz[41], K.Rybicki[18], H.Saarikko[15], Y.Sacquin[39], A.Sadovsky[16], G.Sajot[14], J.Salt[49], J.Sanchez[26], M.Sannino[13], H.Schneider[17], M.A.E.Schyns[52], G.Sciolla[45], F.Scuri[46], Y.Sedykh[16], A.M.Segar[35], A.Seitz[17], R.Sekulin[37], R.C.Shellard[6], I.Siccama[31], P.Siegrist[39], S.Simonetti[39], F.Simonetto[36], A.N.Sisakian[16], B.Sitar[7], T.B.Skaali[33], G.Smadja[25], N.Smirnov[42], O.Smirnova[16], G.R.Smith[37], R.Sosnowski[51], D.Souza-Santos[6], T.Spassov[21], E.Spiriti[40], S.Squarcia[13], H.Staeck[52], C.Stanescu[40], S.Stapnes[33], I.Stavitski[36], K.Stepaniak[51], F.Stichelbaut[9], A.Stocchi[19], J.Strauss[50], R.Strub[10], B.Stugu[4], M.Szczekowski[51], M.Szeptycka[51], T.Tabarelli[28], J.P.Tavernet[23], O.Tchikilev[42], A.Tilquin[27], J.Timmermans[31], L.G.Tkatchev[16], T.Todorov[10], D.Z.Toet[31], A.Tomaradze[2], B.Tome[21], E.Torassa[45], L.Tortora[40], G.Transtromer[24], D.Treille[9],

W.Trischuk[9], G.Tristram[8], A.Trombini[19], C.Troncon[28], A.Tsirou[9], M-L.Turluer[39], I.A.Tyapkin[16], M.Tyndel[37], S.Tzamarias[22], B.Ueberschaer[52], S.Ueberschaer[52], O.Ullaland[9], V.Uvarov[42], G.Valenti[5], E.Vallazza[9], C.Vander Velde[2], G.W.Van Apeldoorn[31], P.Van Dam[31], W.K.Van Doninck[2], J.Van Eldik[31], G.Vegni[28], L.Ventura[36], W.Venus[37], F.Verbeure[2], M.Verlato[36], L.S.Vertogradov[16], D.Vilanova[39], P.Vincent[25], L.Vitale[46], E.Vlasov[42], A.S.Vodopyanov[16], M.Voutilainen[15], V.Vrba[12], H.Wahlen[52], C.Walck[44], F.Waldner[46], A.Wehr[52], M.Weierstall[52], P.Weilhammer[9], A.M.Wetherell[9], D.Wicke[52], J.H.Wickens[2], M.Wielers[17], G.R.Wilkinson[35], W.S.C.Williams[35], M.Winter[10], M.Witek[9], G.Wormser[19], K.Woschnagg[48], K.Yip[35], L.Yu[35], O.Yushchenko[42], F.Zach[25], A.Zaitsev[42], A.Zalewska[18], P.Zalewski[51], D.Zavrtanik[43], E.Zevgolatakos[11], N.I.Zimin[16], M.Zito[39], D.Zontar[43], R.Zuberi[35], G.C.Zucchelli[44], G.Zumerle[36]

[1] Ames Laboratory and Department of Physics, Iowa State University, Ames IA 50011, USA
[2] Physics Department, Univ. Instelling Antwerpen, Universiteitsplein 1, B-2610 Wilrijk, Belgium
and IIHE, ULB-VUB, Pleinlaan 2, B-1050 Brussels, Belgium
and Faculté des Sciences, Univ. de l'Etat Mons, Av. Maistriau 19, B-7000 Mons, Belgium
[3] Physics Laboratory, University of Athens, Solonos Str. 104, GR-10680 Athens, Greece
[4] Department of Physics, University of Bergen, Allégaten 55, N-5007 Bergen, Norway
[5] Dipartimento di Fisica, Università di Bologna and INFN, Via Irnerio 46, I-40126 Bologna, Italy
[6] Centro Brasileiro de Pesquisas Físicas, rua Xavier Sigaud 150, RJ-22290 Rio de Janeiro, Brazil
and Depto. de Física, Pont. Univ. Católica, C.P. 38071 RJ-22453 Rio de Janeiro, Brazil
and Inst. de Física, Univ. Estadual do Rio de Janeiro, rua São Francisco Xavier 524, Rio de Janeiro, Brazil
[7] Comenius University, Faculty of Mathematics and Physics, Mlynska Dolina, SK-84215 Bratislava, Slovakia
[8] Collège de France, Lab. de Physique Corpusculaire, IN2P3-CNRS, F-75231 Paris Cedex 05, France
[9] CERN, CH-1211 Geneva 23, Switzerland
[10] Centre de Recherche Nucléaire, IN2P3 - CNRS/ULP - BP20, F-67037 Strasbourg Cedex, France
[11] Institute of Nuclear Physics, N.C.S.R. Demokritos, P.O. Box 60228, GR-15310 Athens, Greece
[12] FZU, Inst. of Physics of the C.A.S. High Energy Physics Division, Na Slovance 2, 180 40, Praha 8, Czech Republic
[13] Dipartimento di Fisica, Università di Genova and INFN, Via Dodecaneso 33, I-16146 Genova, Italy
[14] Institut des Sciences Nucléaires, IN2P3-CNRS, Université de Grenoble 1, F-38026 Grenoble Cedex, France
[15] Research Institute for High Energy Physics, SEFT, P.O. Box 9, FIN-00014 Helsinki, Finland
[16] Joint Institute for Nuclear Research, Dubna, Head Post Office, P.O. Box 79, 101 000 Moscow, Russian Federation
[17] Institut für Experimentelle Kernphysik, Universität Karlsruhe, Postfach 6980, D-76128 Karlsruhe, Germany
[18] High Energy Physics Laboratory, Institute of Nuclear Physics, Ul. Kawiory 26a, PL-30055 Krakow 30, Poland
[19] Université de Paris-Sud, Lab. de l'Accélérateur Linéaire, IN2P3-CNRS, Bat 200, F-91405 Orsay Cedex, France
[20] School of Physics and Materials, University of Lancaster, Lancaster LA1 4YB, UK
[21] LIP, IST, FCUL - Av. Elias Garcia, 14-1^{o}, P-1000 Lisboa Codex, Portugal
[22] Department of Physics, University of Liverpool, P.O. Box 147, Liverpool L69 3BX, UK
[23] LPNHE, IN2P3-CNRS, Universités Paris VI et VII, Tour 33 (RdC), 4 place Jussieu, F-75252 Paris Cedex 05, France
[24] Department of Physics, University of Lund, Sölvegatan 14, S-22363 Lund, Sweden
[25] Université Claude Bernard de Lyon, IPNL, IN2P3-CNRS, F-69622 Villeurbanne Cedex, France
[26] Universidad Complutense, Avda. Complutense s/n, E-28040 Madrid, Spain
[27] Univ. d'Aix - Marseille II - CPP, IN2P3-CNRS, F-13288 Marseille Cedex 09, France
[28] Dipartimento di Fisica, Università di Milano and INFN, Via Celoria 16, I-20133 Milan, Italy
[29] Niels Bohr Institute, Blegdamsvej 17, DK-2100 Copenhagen 0, Denmark
[30] NC, Nuclear Centre of MFF, Charles University, Areal MFF, V Holesovickach 2, 180 00, Praha 8, Czech Republic
[31] NIKHEF-H, Postbus 41882, NL-1009 DB Amsterdam, The Netherlands
[32] National Technical University, Physics Department, Zografou Campus, GR-15773 Athens, Greece
[33] Physics Department, University of Oslo, Blindern, N-1000 Oslo 3, Norway
[34] Dpto. Fisica, Univ. Oviedo, C/P. Pérez Casas, S/N-33006 Oviedo, Spain
[35] Department of Physics, University of Oxford, Keble Road, Oxford OX1 3RH, UK
[36] Dipartimento di Fisica, Università di Padova and INFN, Via Marzolo 8, I-35131 Padua, Italy
[37] Rutherford Appleton Laboratory, Chilton, Didcot OX11 OQX, UK
[38] Dipartimento di Fisica, Università di Roma II and INFN, Tor Vergata, I-00173 Rome, Italy
[39] Centre d'Etude de Saclay, DSM/DAPNIA, F-91191 Gif-sur-Yvette Cedex, France
[40] Istituto Superiore di Sanità, Ist. Naz. di Fisica Nucl. (INFN), Viale Regina Elena 299, I-00161 Rome, Italy
[41] C.E.A.F.M., C.S.I.C. - Univ. Cantabria, Avda. los Castros, S/N-39006 Santander, Spain, (CICYT-AEN93-0832)
[42] Inst. for High Energy Physics, Serpukov P.O. Box 35, Protvino, (Moscow Region), Russian Federation
[43] J. Stefan Institute and Department of Physics, University of Ljubljana, Jamova 39, SI-61000 Ljubljana, Slovenia
[44] Fysikum, Stockholm University, Box 6730, S-113 85 Stockholm, Sweden
[45] Dipartimento di Fisica Sperimentale, Università di Torino and INFN, Via P. Giuria 1, I-10125 Turin, Italy
[46] Dipartimento di Fisica, Università di Trieste and INFN, Via A. Valerio 2, I-34127 Trieste, Italy
and Istituto di Fisica, Università di Udine, I-33100 Udine, Italy
[47] Univ. Federal do Rio de Janeiro, C.P. 68528 Cidade Univ., Ilha do Fundão BR-21945-970 Rio de Janeiro, Brazil
[48] Department of Radiation Sciences, University of Uppsala, P.O. Box 535, S-751 21 Uppsala, Sweden
[49] IFIC, Valencia-CSIC, and D.F.A.M.N., U. de Valencia, Avda. Dr. Moliner 50, E-46100 Burjassot (Valencia), Spain
[50] Institut für Hochenergiephysik, Österr. Akad. d. Wissensch., Nikolsdorfergasse 18, A-1050 Vienna, Austria
[51] Inst. Nuclear Studies and University of Warsaw, Ul. Hoza 69, PL-00681 Warsaw, Poland
[52] Fachbereich Physik, University of Wuppertal, Postfach 100 127, D-42097 Wuppertal 1, Germany

1 Introduction

The way quarks and gluons transform into hadrons is complex and not entirely understood by present theories. In the current picture the hadronization of a $q\overline{q}$ pair from the decay of a Z^0 is split into 3 phases [1]. In a first phase, gluon emission and parton branching of the original $q\overline{q}$ pair take place. It is believed that this phase can be described by perturbative QCD, although most of the calculations performed today are only to second order. In a second phase, quarks and gluons produced in phase 1 are clustered in colour singlets and transform into mesons and baryons. Only phenomenological models, which need to be tuned to the data, are available to describe this process of fragmentation. The models most frequently used in e^+e^- annihilations are those using string and cluster fragmentation. Most of the primary produced hadrons have very short lifetimes. In the third phase the unstable hadrons decay into hadrons which can be observed or identified by the detector.

A different and purely analytical approach giving quantitative predictions of hadronic spectra are QCD calculations using the so called Modified Leading Logarithmic Approximation (MLLA) under the assumption of Local Parton Hadron Duality (LPHD) [2]. In this model the particle yield is described as function of the variable ξ where $\xi = \ln(1/x_p)$ and x_p is the normalized momentum P_{hadron}/P_{beam}.

$$\frac{1}{\sigma}\frac{d\sigma}{d\xi} = K_{LPHD} \cdot f(\xi, Y, \lambda) \tag{1}$$

with

$$Y = \ln\frac{\sqrt{s}}{Q_0} \quad ; \quad \lambda = \ln\frac{Q_0}{\Lambda_{eff}} \tag{2}$$

The MLLA+LPHD predictions involve three parameters: an effective scale parameter Λ_{eff}, Q_0 as the cut-off parameter in the quark-gluon cascade and an overall normalization factor K_{LPHD} that depends on the particle mass.

In this analysis the $K^{\pm}$ and $p/\overline{p}$ spectra from Z^0 hadronic decays were measured using the Cherenkov signal from the liquid and gas radiator of the DELPHI barrel Ring Imaging CHerenkov (RICH) detector. The measurements were compared to the MLLA+LPHD calculations and to the JETSET 7.3 and HERWIG 5.6 model predictions which use string and cluster fragmentation respectively [3,4].

2 Event and Charged Particle Selection

The analysis presented is based on about 170,000 Z^0 decays, collected with the DELPHI detector equipped with a barrel RICH detector allowing particle identification. The data were taken at a centre-of-mass energy of 91.2 GeV. Apart from the barrel RICH detector the relevant detector components for this analysis were the following tracking chambers: the vertex detector, the inner detector, the time projection chamber and the outer detector. A description of the DELPHI detector and a detailed illustration of the DELPHI RICH detectors can be found in [5,6].

For the event selection charged particles were accepted in the momentum region $0.2 < P < 50$ GeV/c, requiring that the relative momentum error, $\frac{\Delta P}{P}$, was less than 1 and a minimum length of 50 cm was measured in the DELPHI tracking detectors. The charged particle polar angle θ had to be between 20° and 160°. The track impact parameter was

required to be smaller than 5 cm in the plane transverse to the beam and less than 10 cm in the direction of the beam.

A hadronic event was selected by requiring a charged particle multiplicity greater than 4, a total energy deposited by charged particles of at least 15 GeV with at least 3 GeV in each hemisphere. The background, mainly coming from $\tau^+\tau^-$ events, was estimated to be less than 0.2 %.

For the analysis particle identification is essential therefore the charged particle momentum was required to be bigger than 0.7 GeV/c and the polar angle was restricted to the region $41° < \theta < 139°$, which corresponds to the active area of the barrel RICH detector.

3 Evaluation of the Mean Cherenkov Angle

The input for the analysis of the mean Cherenkov angle were single space points measured in the photon detector of the barrel RICH. They correspond to the coordinates of the Cherenkov photo-electrons which were detected and associated to a track. The measured space points were transformed to a plane orthogonal to the track. In this coordinate system the Cherenkov photons from the signal form a ring with the track crossing point in its centre. To perform particle identification a mean Cherenkov angle per track, reflecting the best possible choice from the original single photo-electron distribution was calculated. One of the main difficulties is an efficient separation between noise and signal points. The algorithm to evaluate the mean angle developed for this analysis does not make use of any mass hypothesis [7].

To recognize a circle without making any assumption on its centre, at least three points are needed. Given three points the ring centre and the radius can easily be determined, by constructing a triangle out from the three points and taking the normal at the middle of each side of the triangle. The unique crossing point of the three perpendicular bisectors is the centre of the ring passing through the three original points. This simple triangulation procedure was repeated for all possible three point combinations. For each triangle the ring centre and the radius were recorded. The combinations originating from the signal accumulate their ring centres near the crossing point of the track. Triangles containing noise points spread their centres arbitrarily in position. The mean angle was extracted by fitting the radius distribution of all combinations which have the ring centre in a small cell around the track crossing point. Noise points were efficiently rejected by the combinatorial dominance of the signal. Given n points on a circle the density in the cell around the centre grows as $n(n-1)(n-2)/6$ [7].

After the calculation of the mean Cherenkov angle the number of signal photo-electrons (n_{sig}) was determined for this track, as the number of photo-electrons which satisfy: $|\theta_j - \theta| < 3 \cdot \Delta\theta_j$, where θ_j is the Cherenkov angle of the individual photo-electron j, $\Delta\theta_j$ is the error of θ_j and θ is the mean Cherenkov angle for this track. The error on the mean angle $\Delta\theta$ is obtained from the width of the corresponding radius distribution divided by $\sqrt{n_{sig}}$.

Further cuts were applied in order to optimize particle identification. It was required that the photon detector traversed by the particle recorded its ionization, thus assuring that the corresponding sector of the detector was operational. The number of signal photo-electrons assigned to the ring was required to be greater than 5 in the liquid radiator and greater than 3 in the gas radiator. The error of the mean angle $\Delta\theta$ was required to be less than 0.011 rad for rings from the liquid radiator. With these additional quality cuts between 57 % and 93 % of the tracks crossing the barrel RICH in the liquid

and between 45 % and 65 % in the gas were retained, where the efficiencies rise with increasing momenta.

4 Measurement of Inclusive $K^{\pm}$ and $p/\overline{p}$ Rates

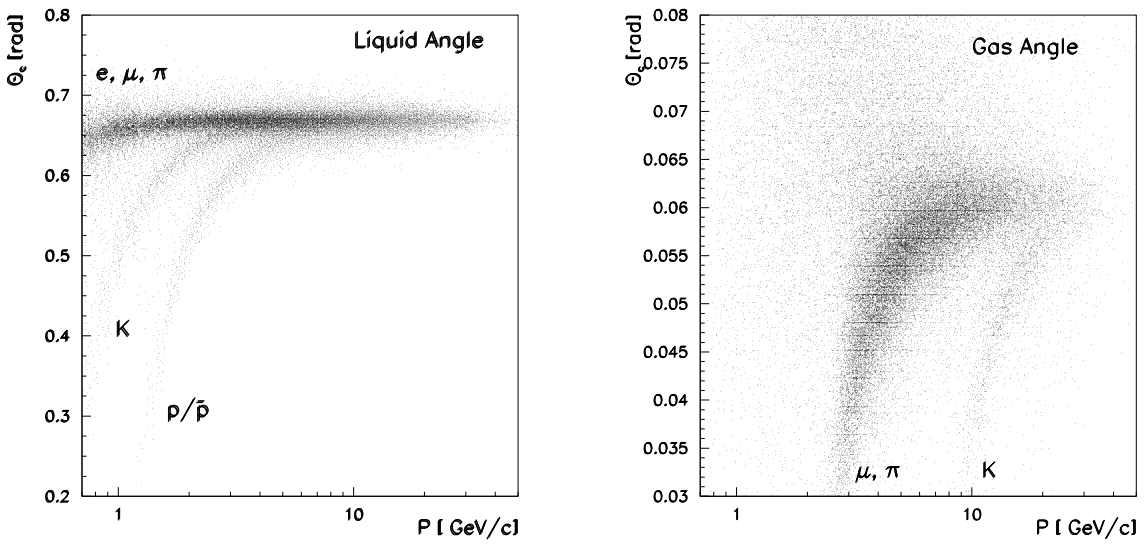

(a) (b)

Figure 1: Cherenkov angle versus the charged particle momentum in (a) the liquid radiator and (b) the gas radiator.

For a given momentum, the Cherenkov angle depends on the mass of the particle and the refractive index of the radiator. Figures 1 to 3 show the Cherenkov angles reconstructed with the triangulation method for liquid and gas radiator. For the gas radiator (see Figure 1(b)) an accumulation of background at large angles and small momenta is observed which is mainly due to scattered tracks, especially electrons, and veto particles accompanied with noise points. A veto particle is such that its velocity is below the threshold for Cherenkov light emission in the relevant medium. The fraction of $K^{\pm}$ and $p/\overline{p}$ were extracted using a maximum likelihood fit for the Cherenkov angle distribution in discrete momentum intervals. For each track satisfying the selection criteria, the probability density "l_i" of observing the measured angle θ_i was calculated.

$$l_i = \frac{1}{C} \cdot \left[\frac{(1-f_K-f_p)}{\Delta\theta_i^{\pi}} \cdot e^{-\frac{(\theta_i-\theta^{\pi})^2}{2(\Delta\theta_i^{\pi})^2}} + \frac{f_K}{\Delta\theta_i^{K}} \cdot e^{-\frac{(\theta_i-\theta^{K})^2}{2(\Delta\theta_i^{K})^2}} + \frac{f_p}{\Delta\theta_i^{p}} \cdot e^{-\frac{(\theta_i-\theta^{p})^2}{2(\Delta\theta_i^{p})^2}} + b \right] \quad (3)$$

with

θ_i	: measured Cherenkov angle of track i
$\theta^{\pi,K,p}$	: expected Cherenkov angle for a pion†, kaon and proton
$\Delta\theta_i^{\pi,K,p}$	: $= \sqrt{\Delta\theta^2 + (\frac{\partial\theta}{\partial P}\Delta P)^2}$ error on the Cherenkov angle of track i for a pion, kaon and proton

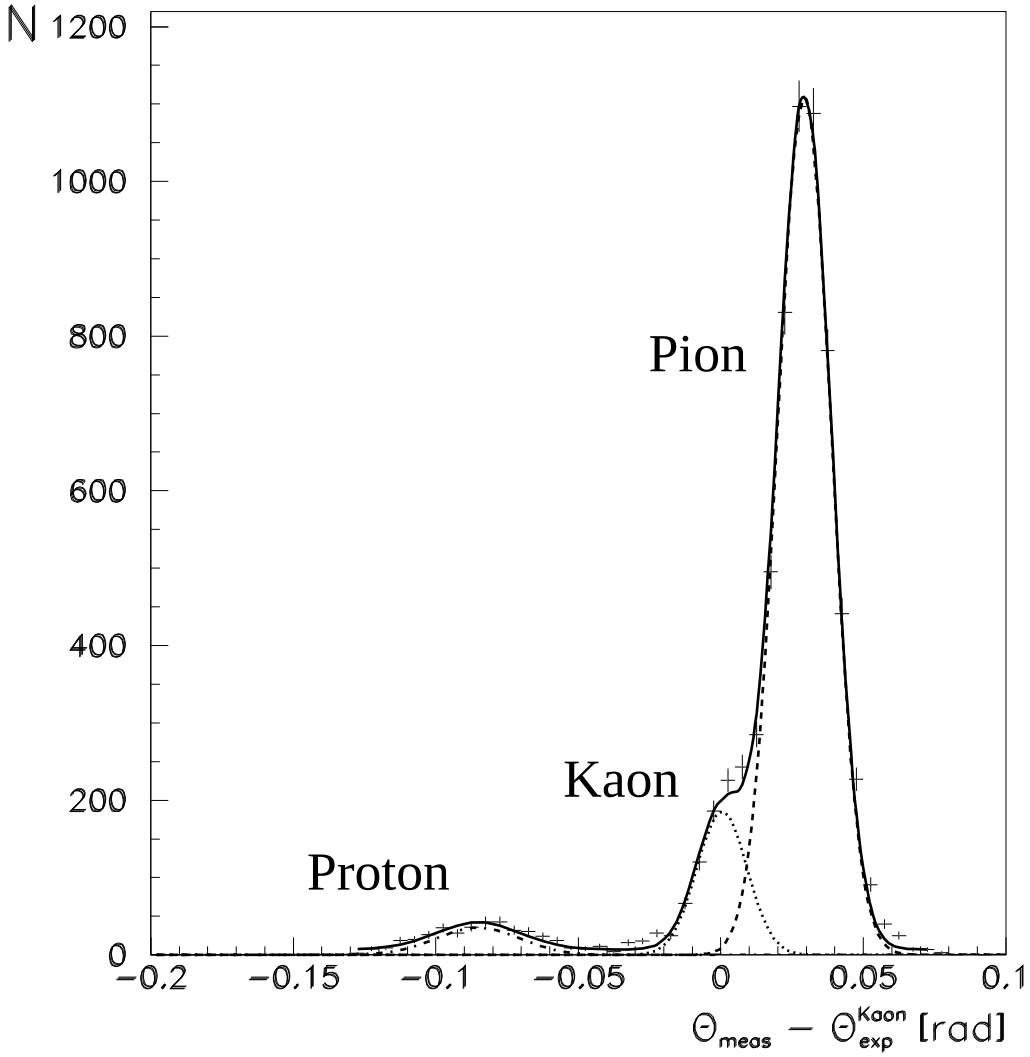

Figure 2: Cherenkov angle distribution in multi-hadronic events for the momentum interval $2.0 < P < 2.5$ GeV/c. Plotted is $\theta_{meas} - \theta_{exp}^{kaon}$ of the liquid radiator signal, the full lines corresponds to a fit of three Gaussians plus a flat background.

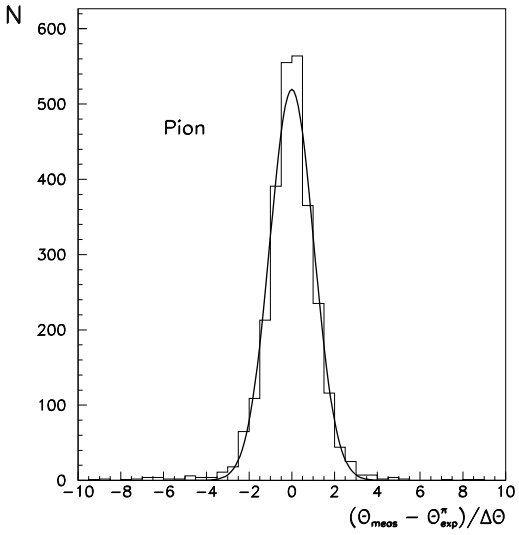

(a)

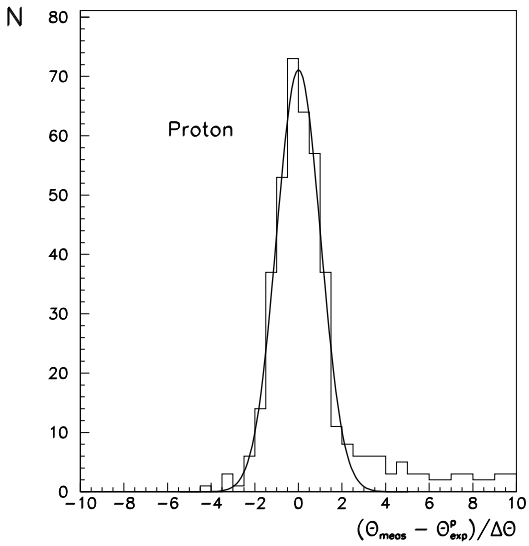

(b)

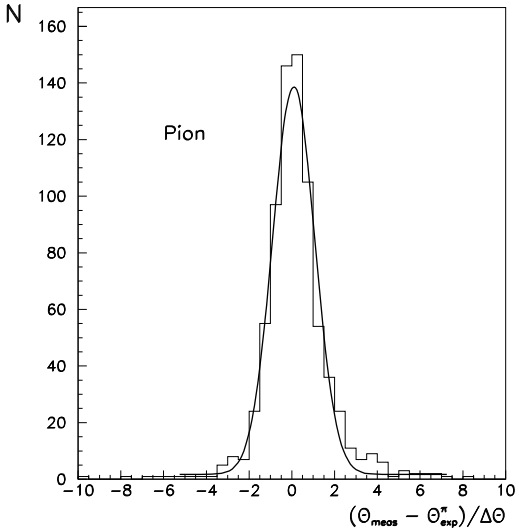

(c)

Figure 3: Distribution of the normalized angle $\frac{\theta-\theta_{exp}}{\Delta\theta}$ using (a) identified pions from K^0 decays for the liquid radiator signal, (b) identified protons from Λ^0 decays for the liquid radiator signal and (c) identified pions from K^0 decays for the gas radiator signal. In (b) the background on the right hand side of the distribution is due to residual pion contamination in the proton sample.

f_K : fraction of kaons estimated by the fit
f_p : fraction of protons estimated by the fit
b : constant for the background
C : normalization constant

Normally particles which do not have an appropriate Cherenkov angle measurement were removed by the quality cuts, but badly measured tracks may sometimes have passed the cuts and contributed to the background. Hence the background term b contains apart from real background such as veto particles or digitizations from multiple scattering also some $\pi^{\pm}$, $K^{\pm}$ and $p/\overline{p}$. But Figures 2 and 3 show that the fitted distributions contain only little background which justifies the approach $b = constant$.

The normalization constant C was determined through the integral

$$1 = \int_{\theta_1(P_{low})}^{\theta_2(P_{up})} l_i(f_K, f_p, \theta_i, \Delta\theta_i, b)\, d\theta \tag{4}$$

where the integration limits θ_1 and θ_2 cover, for the liquid radiator, the range from $\theta_1(P_{low}) = \theta_{prot.} - 0.060$ rad and $\theta_2(P_{up}) = \theta_{elec.} + 0.060$ rad, taking for $P_{low}(P_{up})$ the lower (upper) limit of each fitted momentum interval. For the gas radiator the integration covers the entire active θ range from 0 to 70 mrad.

The extended likelihood function $\mathcal{L}_E$ in eqn.(5) is derived from the product of the l_i over all tracks and an additional Poissonian factor estimating the probability of obtaining a sample of size ψ [8].

$$\mathcal{L}_E = \frac{\psi^m \cdot e^{-\psi}}{m!} \prod_{i=1}^{m} l_i(f_K, f_p, \theta_i, \Delta\theta_i, b) \tag{5}$$

m : total number of entries in the given momentum bin
ψ : total number of tracks (including background) estimated by the fit

$\mathcal{L}_E$ describes the probability to obtain the observed sample of measurements. The parameters ψ, f_K, f_p and b were estimated by maximizing the logarithm of the likelihood function in equation (5).

The upper kinematical limit to which the different particle types can be separated depends crucially on the distances $\frac{\theta_\pi - \theta_K}{\sqrt{2}\Delta\theta}$ and $\frac{\theta_K - \theta_p}{\sqrt{2}\Delta\theta}$, which are shown in Figure 4. Requiring a minimal separation of $\frac{\theta_{\pi(K)} - \theta_{K(p)}}{\sqrt{2}\Delta\theta} \gtrsim 0.8$ and taking into account the behaviour of the systematic errors (see section 4.1) the kaon fraction was extracted from the measurement up to 4.0 GeV/c in the liquid and up to 23 GeV/c in the gas radiator. For the proton fraction, the limit in the liquid radiator was 5 GeV/c.

In this analysis a fit for the measured Cherenkov angle was used, therefore the lower kinematical limit is given by the Cherenkov threshold $P \geq \sqrt{\frac{M^2}{n^2-1}}$ which depends on the mass M and the refractive index n. To keep efficiency corrections small (discussed in section 4.1), the following lower momentum limits were used: in the liquid $P_{low}^{kaon} = 0.8$ GeV/c and $P_{low}^{proton} = 1.4$ GeV/c, in the gas only the kaon yield for $P_{low}^{kaon} = 10.0$ GeV/c was evaluated. In order to estimate the proton fraction at high momenta it is favorable to take advantage of the veto signal. This requires an extension in eqn.(3) for the probability of observing no light at all, which was not done for this analysis. The veto signal would allow a determination of the proton rate for $P \gtrsim 10$ GeV/c.

[†]Pion stands for pion, electron or muon since they cannot be distinguished in most cases.

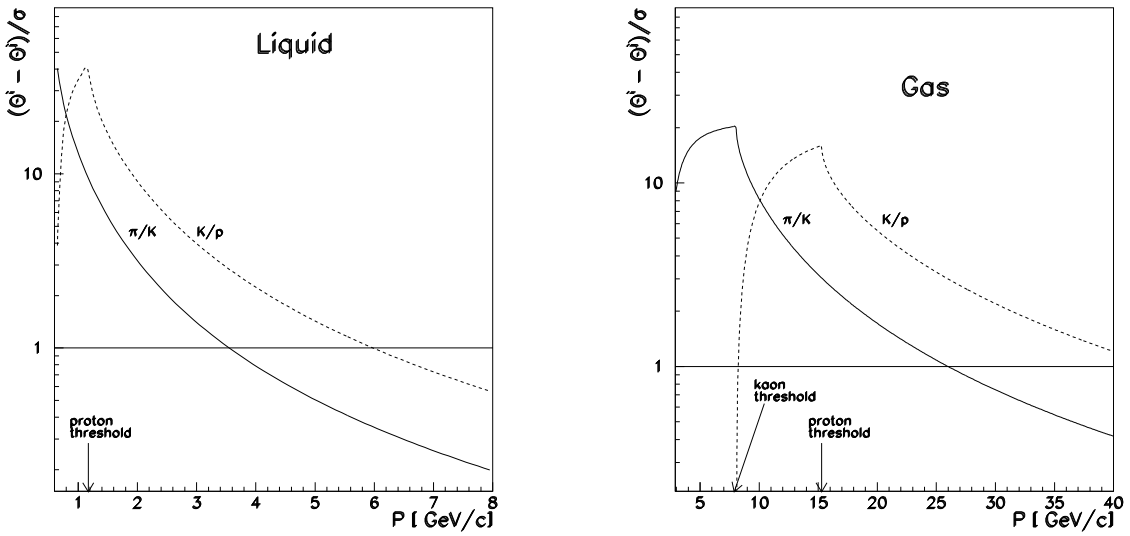

(a) (b)

Figure 4: The hadron separation capacities $\frac{\theta_\pi - \theta_K}{\sigma}$ and $\frac{\theta_K - \theta_p}{\sigma}$ with $\sigma = \sqrt{2}\Delta\theta$ are shown for (a) the liquid and (b) for the gas radiator. Full curve is pion/kaon separation and dashed curve is kaon/proton separation.

In some of the low momentum intervals the proton is below or very close to its threshold for emitting Cherenkov light (veto particle). Protons are therefore excluded from the probability density in eqn.(3). In this case a correction factor to the number of tracks measured was applied using the proton yield predicted by JETSET. Using the proton yield measured in [9], which is significantly lower than the JETSET fraction at high momenta, would change the results by an amount much smaller than the experimental errors.

4.1 Efficiency and Acceptance Corrections and Systematic Error Evaluation

Some long lived particles such as K^0_S, K^0_L or Λ^0 may or may not decay inside the detector. The measurements were corrected such that all K^0_S and Λ^0 decay products were included and all K^0_L were counted as stable particles. Furthermore the fractions were corrected bin by bin for detector effects and particles produced in secondary interactions. Both corrections were evaluated using the full DELPHI detector simulation [10].

It is important to take account of any relative efficiency differences between particle species. The number of photo-electrons in a ring is proportional to $\sin^2\theta$. Considering a momentum interval where particles with different masses have distinct Cherenkov angles, less photo-electrons are expected for heavier particles than for lighter ones. This leads to a lower ring detection efficiency in some of the lower momentum bins for kaons or protons with respect to pions. Since eqn.(3) does not include a term which corrects for efficiency differences depending on the number of photo-electrons, this effect was treated

separately. The procedure to correct the measured fractions was different for rings from the liquid and from the gas radiator.

In the rings from the liquid radiator, for pions and protons, the efficiencies can be measured using identified tracks from K^0 or Λ decays. In Figure 5 (a) the efficiency to find a ring at the expected position with the selection criteria used in this analysis is plotted as a function of the momentum. The difference between pion and proton efficiency at low momenta is due to the reduced number of photo-electrons in the proton ring. The proton efficiency correction can be extracted bin by bin from the ratio of $\frac{\varepsilon_p}{\varepsilon_\pi}$. Very good agreement is observed for the extracted efficiency ratio between data and simulation. (see Figure 5 (b)). The efficiency corrections for kaons and protons were therefore estimated using detector simulation. A minimal error of $\pm$ 5% on the efficiency correction was assumed if the statistical error from the simulation was smaller (Table 1).

In the rings from the gas radiator, particles with an equal number of photo-electrons are expected to have the same ring detection efficiency. However, there are arguments for a kaon at 12 GeV/c not to have the same efficiency as a pion at 3.5 GeV/c: they have different momentum errors, they have different densities of surrounding tracks and the track curvature in the radiator is different. Despite these additional factors, the simulation predicts similar reconstruction efficiencies for pions and kaons with equal number of photo-electrons. This result is because the ring detection efficiency does not depend strongly on the resolution of the Cherenkov angle but rather on the number of photo-electrons. In Figure 5 (c) the efficiencies are shown versus the relative number of photo-electrons in the ring, which is defined as the measured number divided by the number of photo-electrons obtained in a ring with the maximal Cherenkov angle. In the data, the ring detection efficiency can be measured for pions from K^0 decays (Figure 5 (d)). Using the above arguments, the kaon efficiency was assumed to be equal to the pion efficiency for the same number of photo-electrons ($\varepsilon_K(n_K) = \varepsilon_\pi(n_\pi)$ for $n_\pi = n_K$). The corrections are given in Table 2. They are in agreement with the relative efficiency corrections which were extracted from the simulation directly.

Momentum	Correction Factor	
Interval [GeV/c]	Kaon	Proton
0.8 - 1.1	1.18 $\pm$ 0.06	-
1.1 - 1.4	1.02 $\pm$ 0.05	-
1.4 - 1.7	1.00 $\pm$ 0.05	1.96 $\pm$ 0.15
1.7 - 2.0	1.00 $\pm$ 0.05	1.27 $\pm$ 0.09
2.0 - 2.5	1.00 $\pm$ 0.05	1.17 $\pm$ 0.07
2.5 - 3.0	1.00 $\pm$ 0.05	1.09 $\pm$ 0.08

Table 1: Efficiency correction factors in the Cherenkov liquid for kaons and protons due to differences in the number of photo-electrons.

The uncertainties due to differences in efficiency between different particles were directly obtained from the errors on the correction factors given in Tables 1 and 2 and they appear in column 5 of Tables 3 and 4. Where no efficiency correction was applied, a 5% relative systematic error was assumed.

The expected Cherenkov angles for the different particles were used as input to the fitting procedure and kept constant during the fit. Errors in these quantities contribute to the systematic error. To evaluate this contribution the fitting procedure was repeated with a systematic shift in the expected Cherenkov angle of $\pm$0.5 mrad in the liquid, and $\pm$0.2 mrad in the gas. These variations were computed for all momentum bins and the

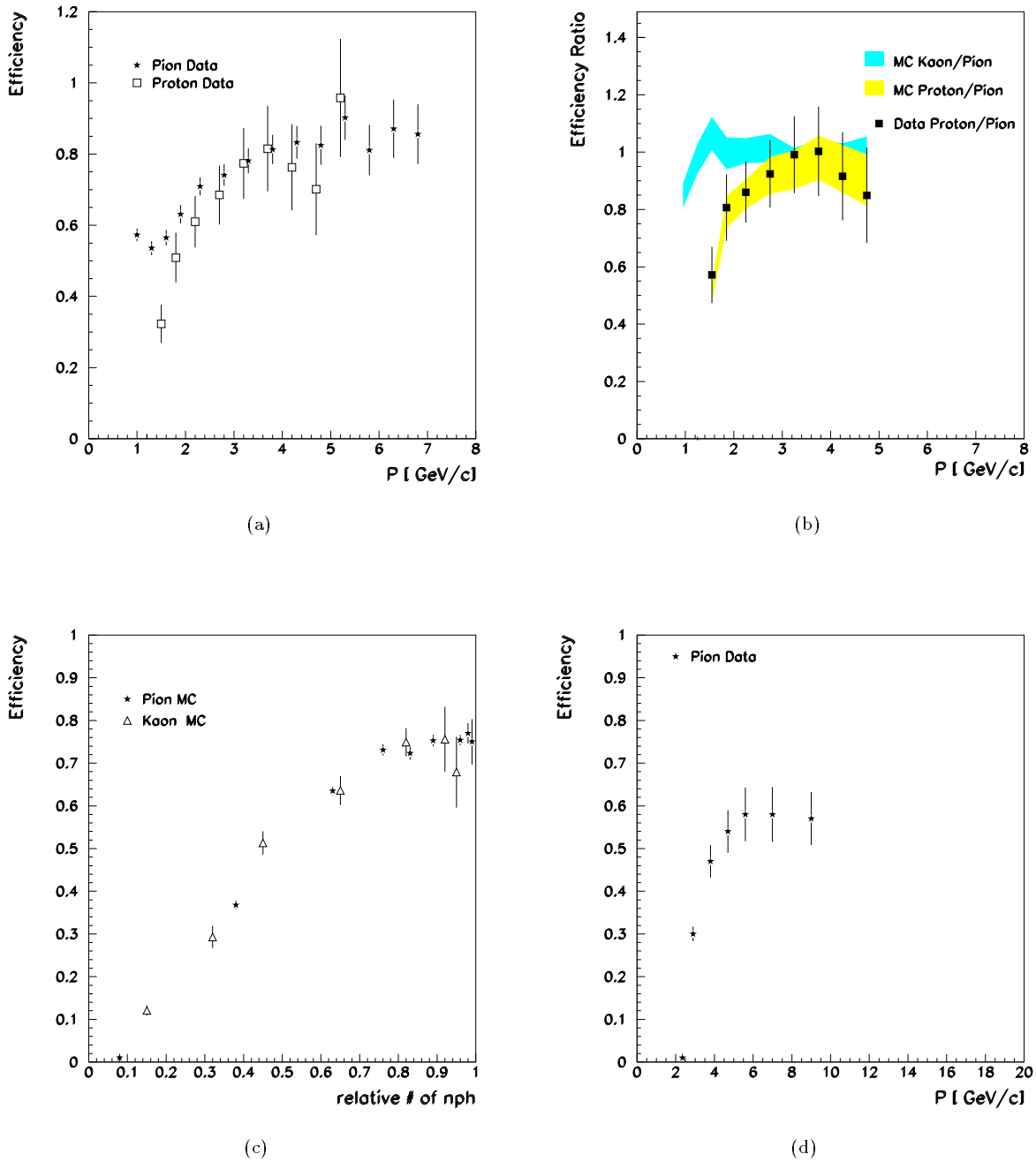

Figure 5: Ring detection efficiencies in (a,b) the liquid radiator and (c,d) the gas radiator. (a) Efficiencies for pions and protons measured in the data, (b) efficiency ratios $\frac{\varepsilon_K}{\varepsilon_\pi}$ and $\frac{\varepsilon_p}{\varepsilon_\pi}$ in the simulation (shaded areas) and in the data (points), (c) efficiencies as a function of the relative number of photo-electrons and (d) pion efficiency measured in the data.

Momentum Interval [GeV/c]	Correction Factor Kaon
10.0 - 12.0	1.70 ± 0.29
12.0 - 14.0	1.28 ± 0.08
14.0 - 16.0	1.15 ± 0.07
16.0 - 18.0	1.11 ± 0.05
18.0 - 20.0	1.07 ± 0.05
20.0 - 23.0	1.03 ± 0.05

Table 2: Efficiency correction factors in the Cherenkov gas for kaons due to differences in the number of photo-electrons.

change in the fraction observed was taken as the contribution to the systematic error which is given in column 6 of Tables 3 and 4. This error is negligible in the region where the angular separation is large.

In the liquid radiator signal, in some cases, a small non-Gaussian tail towards smaller values in the Cherenkov angle distribution was observed. This tail was caused by a few poorly measured particles. The procedure used to evaluate the systematic errors shown in column 7 of Tables 3 and 4 uses pions identified in the gas radiator. Tight identification cuts on the gas radiator signal allow pion selection with a purity near 100 % in the momentum range from 2.5 to 8.0 GeV/c. This pion sample allows to fit single particle distribution in the liquid with the likelihood function in all momentum bins above 2.5 GeV/c. The number of kaons determined from the fit were used to extract the systematic error contribution on the kaon fraction due to pions. For the protons the main influence comes from the tail originating from the nearby kaon distribution. Therefore the measured pion angle was shifted such that it appears on the position of the kaon peak and the same procedure was repeated. The shape errors for $P < 2.5$ GeV/c can be neglected since the pion, kaon and proton curves have very little overlap in this kinematical range.

5 Results

With the methods described in the previous section a large fraction of the possible error sources are covered and a conservative error estimation on the inclusive kaon and proton fractions is obtained. In Tables 3 and 4, a complete summary of the measured fractions with their statistical and systematic errors is given. The three sources of systematic errors which were discussed before and the error resulting from the likelihood fit are listed in all relevant momentum intervals. The fit error is essentially the statistical error. The total systematic error, which is calculated from the quadratic sum of the three single systematic errors, is also given. In Figure 6 the $K^{\pm}$ and $p/\overline{p}$ fractions are shown and compared to the JETSET 7.3 and HERWIG 5.6 models. The kaon fraction in the low momentum region is well represented by the JETSET model, while at higher momenta there is some indication of a higher kaon yield in the data. The proton fraction in the JETSET model is up to 15 % higher than in the data, while the HERWIG model is in good agreement with the proton yield in the measured kinematical region.

The differential $K^{\pm}$ and $p/\overline{p}$ cross-sections were obtained by multiplying the measured fraction with the total cross-section for charged particles. Figure 7 shows that the total charged spectrum is in excellent agreement with the predictions from JETSET 7.3. The differential cross-sections for $K^{\pm}$ and $p/\overline{p}$ are summarized in Table 5 as functions of x_p

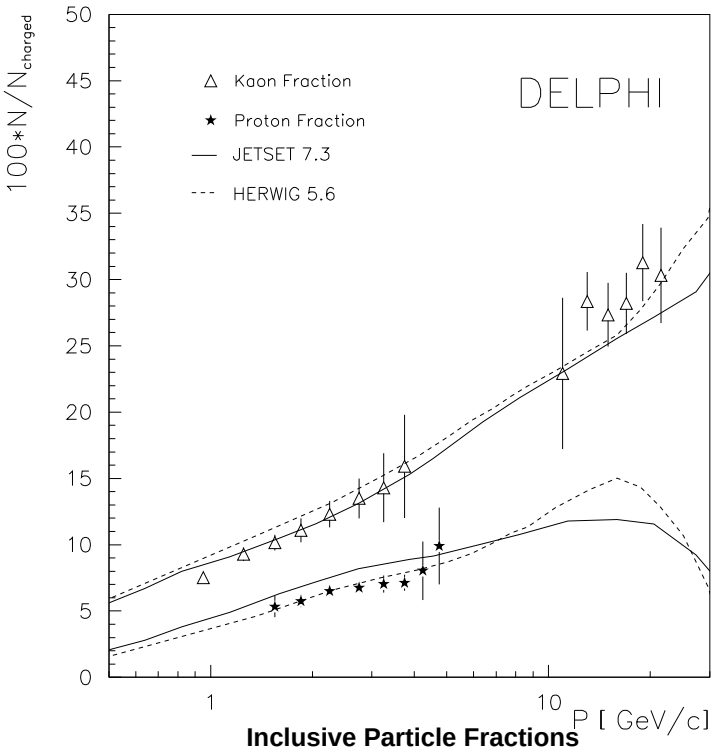

Figure 6: The measured percentages of $K^{\pm}$ and $p/\overline{p}$ among all charged particles are shown with their total errors.

Momentum Interval [GeV/c]	$< P >$ [GeV/c]	Kaon Fraction [%]	Fit Error	Systematic Errors Eff.	Angle	Shape	Total
0.8 - 1.1	0.95	7.5	± 0.14	± 0.4	< 0.1	–	± 0.4
1.1 - 1.4	1.25	9.3	± 0.24	± 0.4	< 0.1	–	± 0.4
1.4 - 1.7	1.55	10.2	± 0.29	± 0.5	< 0.1	–	± 0.5
1.7 - 2.0	1.85	11.1	± 0.32	± 0.6	< 0.3	< 0.5	± 0.8
2.0 - 2.5	2.25	12.3	± 0.35	± 0.6	± 0.5	< 0.5	± 0.9
2.5 - 3.0	2.75	13.5	± 0.40	± 0.6	± 1.1	± 0.7	± 1.4
3.0 - 3.5	3.25	14.3	± 0.48	± 0.6	± 1.9	± 1.5	± 2.5
3.5 - 4.0	3.75	15.9	± 0.60	± 0.8	± 3.0	± 2.3	± 3.9
10 - 12	11.0	22.9	± 1.5	± 5.5	< 0.5	-	± 5.5
12 - 14	13.0	28.4	± 0.5	± 2.1	< 0.5	-	± 2.2
14 - 16	15.0	27.4	± 0.7	± 2.2	± 0.7	-	± 2.3
16 - 18	17.0	28.2	± 0.9	± 1.5	± 1.5	-	± 2.1
18 - 20	19.0	31.3	± 1.1	± 1.6	± 2.2	-	± 2.7
20 - 23	21.5	30.3	± 1.2	± 1.6	± 3.0	-	± 3.4

Table 3: Inclusive kaon percentages and their errors measured in the liquid (low momenta) and in the gas (high momenta).

Momentum Interval [GeV/c]	$< P >$ [GeV/c]	Proton Fraction [%]	Fit Error	Systematic Errors Eff.	Angle	Shape	Total
1.4 - 1.7	1.55	5.3	± 0.20	± 0.8	< 0.1	–	± 0.8
1.7 - 2.0	1.85	5.8	± 0.22	± 0.4	< 0.1	–	± 0.4
2.0 - 2.5	2.25	6.5	± 0.25	± 0.3	± 0.1	–	± 0.3
2.5 - 3.0	2.75	6.8	± 0.25	± 0.3	± 0.1	< 0.1	± 0.3
3.0 - 3.5	3.25	7.0	± 0.25	± 0.4	± 0.1	± 0.4	± 0.6
3.5 - 4.0	3.75	7.1	± 0.27	± 0.4	± 0.1	± 0.3	± 0.5
4.0 - 4.5	4.25	8.0	± 0.30	± 0.4	± 0.7	± 2.0	± 2.2
4.5 - 5.0	4.75	9.9	± 0.38	± 0.5	± 1.3	± 2.5	± 2.9

Table 4: Inclusive proton percentages and their errors measured in the liquid.

and momentum, P. The mean $K^{\pm}$ multiplicity per hadronic event was evaluated using a fit through the data in the range of $0.018 < x_p < 0.5$ which corresponds to 79 % of the full integral. In the unmeasured region the kaon fraction was extrapolated using the JETSET prediction. This leads to a mean multiplicity per Z^0 decay of:

$$< N_{K^{\pm}} > = \; 2.26 \pm 0.01\,(stat.) \pm 0.16\,(sys.) \pm 0.09\,(extrapol.) \qquad (6)$$

The error is split in 3 parts: statistical error, systematic error from the measurement and a systematic error from the extrapolation which was assumed to be $\pm$ 20%. For the $p/\overline{p}$ the measured range of $0.031 < x_p < 0.11$ covers only $\sim$ 50% of the full integral. In the measured region alone the multiplicity is $\sim$ 10.5% lower than in JETSET. The extrapolation to the full x_p range assuming a total production which is 10.5% lower than JETSET leads to a value of:

$$< N_{p/\overline{p}} > = \; 1.07 \pm 0.01\,(stat.) \pm 0.05\,(sys.) \pm 0.13\,(extrapol.) \qquad (7)$$

The results are consistent with a measurement from the OPAL collaboration [9], where the $\pi^{\pm}$, $K^{\pm}$ and $p/\overline{p}$ yields were obtained from an energy loss measurement in the OPAL jet chamber. By overlaying the $p/\overline{p}$ measurements from DELPHI, the proton yield is determined over the full kinematical range. Both measurements see a lower $p/\overline{p}$ yield, than given by JETSET 7.3.

QCD calculations within the framework of the Modified Leading Logarithm Approximation (MLLA) and Local Parton Hadron Duality (LPHD) make predictions of inclusive hadronic spectra in $\xi = \ln(1/x_p)$ [2]. The calculation predicts that the momentum fraction distribution has the form of a "humped-backed-plateau", which is approximately Gaussian in ξ [11]. In order to compare the MLLA predictions with the data, the data can be fitted with a simple Gaussian in the peak region only or with a distorted Gaussian over the entire spectrum, as proposed in [12]. The formula for the distorted gaussian used was

$$D(N, <\xi>, \sigma, \delta, s, k) = \frac{N}{\sigma\sqrt{2\pi}}\; \exp\left(\frac{1}{8}k - \frac{1}{2}s\delta - \frac{1}{4}(2+k)\delta^2 + \frac{1}{6}s\delta^3 + \frac{1}{24}k\delta^4\right) \qquad (8)$$

where N is an overall normalization factor, $\delta = \frac{\xi - <\xi>}{\sigma}$ with $<\xi>$ being the peak position in leading order, σ is the width, s the skewness and k the kurtosis of the distribution.

In Figure 8 the measured distributions $\frac{1}{\sigma_{had}}\frac{d\sigma}{d\xi}$ for $K^{\pm}$ and $p/\overline{p}$ are shown. The maxima (ξ^*) of the distributions were determined to be 2.63 ± 0.07 and 2.96 ± 0.16 for $K^{\pm}$ and $p/\overline{p}$ respectively. The kaon distribution was fitted with a distorted Gaussian function. A Gaussian function was used to determine the ξ^*-value for the proton distribution.

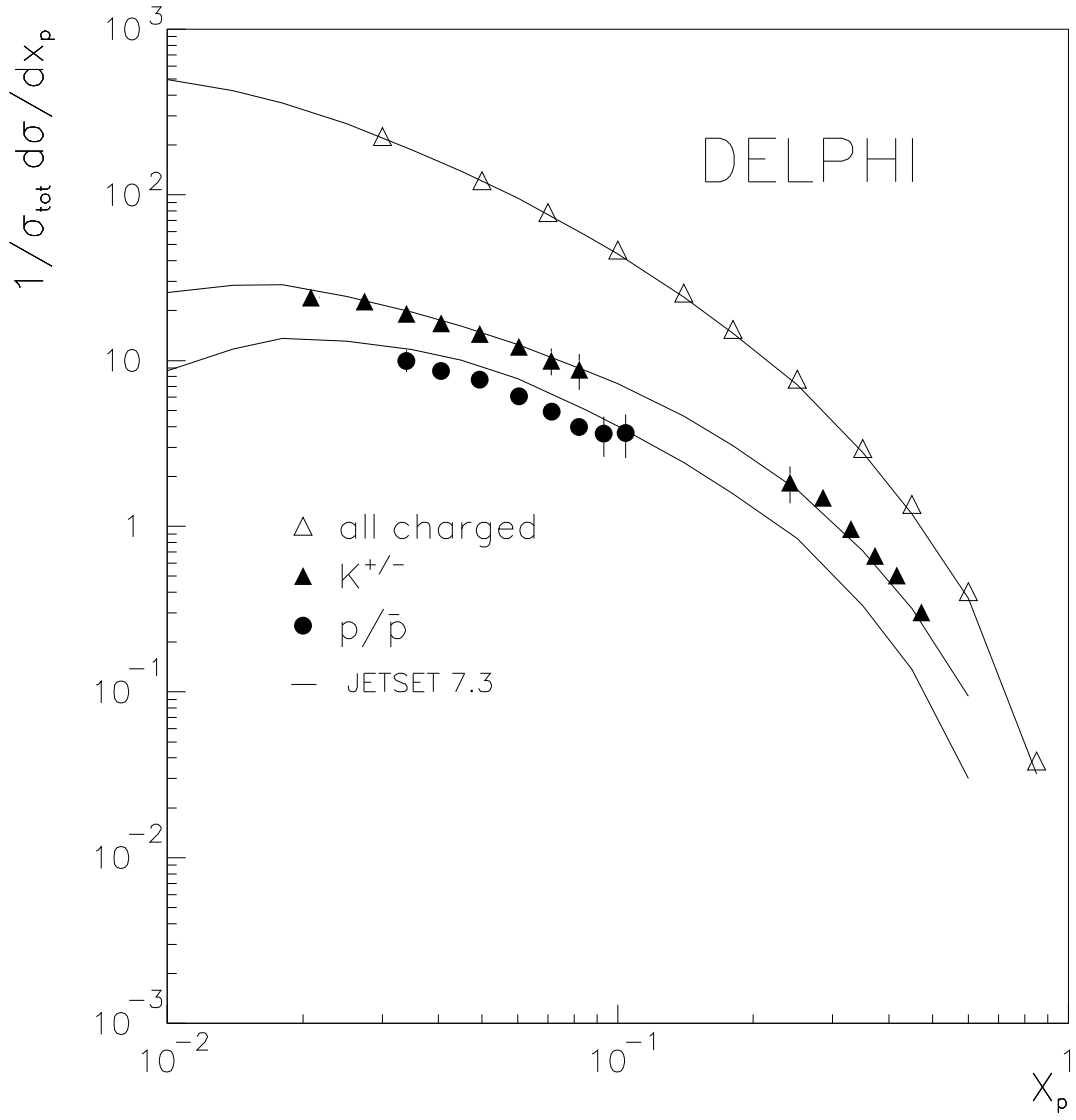

Figure 7: Differential cross-sections for inclusive $K^{\pm}$ and $p/\overline{p}$ production as functions of normalized momentum x_p. Points are measured values, also showing errors, lines are predictions of the JETSET 7.3 model.

Momentum [GeV/c]	$< x_p >$	$\frac{1}{\sigma_{had}}\frac{d\sigma_K}{dx_p}$	$\frac{1}{\sigma_{had}}\frac{d\sigma_K}{dP}$ $[\mathrm{GeV/c}]^{-1}$	$\frac{1}{\sigma_{had}}\frac{d\sigma_p}{dx_p}$	$\frac{1}{\sigma_{had}}\frac{d\sigma_p}{dP}$ $[\mathrm{GeV/c}]^{-1}$
0.8 - 1.1	0.021	23.9 ± 1.27	0.524 ± 0.028		
1.1 - 1.4	0.028	22.8 ± 1.23	0.500 ± 0.027		
1.4 - 1.7	0.034	19.1 ± 1.13	0.419 ± 0.025	10.0 ± 1.50	0.219 ± 0.033
1.7 - 2.0	0.041	16.7 ± 1.36	0.366 ± 0.030	8.69 ± 0.76	0.191 ± 0.017
2.0 - 2.5	0.050	14.5 ± 1.18	0.318 ± 0.026	7.63 ± 0.47	0.167 ± 0.010
2.5 - 3.0	0.061	12.1 ± 1.35	0.265 ± 0.030	6.06 ± 0.36	0.133 ± 0.008
3.0 - 3.5	0.072	10.0 ± 1.82	0.219 ± 0.040	4.91 ± 0.45	0.108 ± 0.010
3.5 - 4.0	0.083	8.8 ± 2.16	0.193 ± 0.047	3.95 ± 0.33	0.087 ± 0.007
4.0 - 4.5	0.094			3.60 ± 0.99	0.079 ± 0.022
4.5 - 5.0	0.106			3.66 ± 1.07	0.080 ± 0.023
10 - 12	0.241	1.833 ± 0.456	0.0402 ± 0.0100		
12 - 14	0.285	1.483 ± 0.115	0.0325 ± 0.0025		
14 - 16	0.329	0.960 ± 0.084	0.0211 ± 0.0018		
16 - 18	0.373	0.663 ± 0.054	0.0145 ± 0.0012		
18 - 20	0.417	0.507 ± 0.047	0.0111 ± 0.0010		
20 - 23	0.471	0.303 ± 0.036	0.0067 ± 0.0008		

Table 5: $\mathrm{K}^{\pm}$ and $\mathrm{p}/\overline{\mathrm{p}}$ cross-sections depending on x_p and P.

The peak values from single particle distributions and their dependence on the hadron mass are of interest. In the framework of MLLA+LPHD smaller peak values are expected for more massive particles [15]. A complete list of the measured ξ^*-values with their errors is given in Table 6. Most ξ^*-values were directly taken from the references given in the last column, for the rows marked with an "$*$" the fit of the ξ-distribution, determining the ξ^*-value, was carried out in the presented analysis. The errors contain the quadratic sum of the statistical error from the fit and the systematic error from variations of the fit conditions. The data indicate a different mass dependence of ξ^* for mesons and baryons. Figure 9 shows the measured ξ^*-position for $\mathrm{K}^{\pm}$ and $\mathrm{p}/\overline{\mathrm{p}}$ combined with various other measurements at LEP.

At LEP energies the majority of the observed hadrons come from secondary decays of heavier primary hadrons. Using the latest (1994) DELPHI tuning of the JETSET 7.3 model, which generally reproduces well the known particle spectra, the influence of particle decays on the observed ξ^*-positions was estimated. This was done by comparing the peak values with and without inhibiting all particles decays. The quantity $\Delta\xi^*_{\mathrm{decays}}$, defined in equation 9, was added to the measured ξ^*-values.

$$\xi^*_{\mathrm{prim}} = \xi^* + \Delta\xi^*_{\mathrm{decays}} \tag{9}$$

In Figure 10 (a) the corrected ξ^*_{prim}-positions for primary hadrons are shown. The full line is a fit proportional to $-\log(M_{hadron})$ which describes the data satisfactorily. In the MLLA calculations the peak position moves linearly with $-\log(\frac{Q_0}{\Lambda})$ [17] with Q_0 being the cut-off parameter in the parton cascade and Λ an effective QCD scale. Q_0 is related to the hadron mass, where the most simple approach is $Q_0 \approx M_{hadron}$ [2], thus leading to a linear dependence between ξ^*_{prim} and $-\log(M_{hadron})$. The errors on the decay corrections ($\Delta\xi^*_{\mathrm{decays}}$) were estimated through variation of relevant JETSET parameters and are typically 10-20% of the applied correction. Figure 10 (b) shows that the decay corrections vary quantitatively for the different particle species and are relatively large for $\mathrm{K}^{\pm}$, K^0 and K^{*0}. The corrected ξ^*_{prim}-values show a smooth decrease with increasing

hadron mass, which is in good agreement with the expectation of the MLLA+LPHD model (Figure 10).

Particle	ξ^*	$\Delta\xi^*_{\rm decays}$	Fit Function	Experiment	Reference
π^0	3.96 $\pm$ 0.13	-0.22	limited spectrum	L3	[18]
$\pi^\pm$	3.81 $\pm$ 0.02	-0.22		OPAL	[9]
$\pi^\pm$	3.78 $\pm$ 0.02		Gaussian	ALEPH	[20]
$K^\pm$	2.70 $\pm$ 0.09	0.54	Gaussian	ALEPH	[20]
$K^\pm$	2.63 $\pm$ 0.07		distorted Gaussian *	DELPHI	this paper
$K^\pm$	2.63 $\pm$ 0.04			OPAL	[9]
K^0	2.65 $\pm$ 0.05	0.41	distorted Gaussian *	ALEPH	[19]
K^0	2.57 $\pm$ 0.08		distorted Gaussian *	DELPHI	[13]
K^0	2.89 $\pm$ 0.05		limited spectrum	L3	[18]
K^0	2.77 $\pm$ 0.05		distorted Gaussian *	OPAL	[21]
η	2.52 $\pm$ 0.10	0.13	limited spectrum	L3	[18]
K^{*0}	2.51 $\pm$ 0.20	0.58	Gaussian	OPAL	[22]
$p/\overline{p}$	2.85 $\pm$ 0.18	0.11	Gaussian	ALEPH	[20]
$p/\overline{p}$	2.96 $\pm$ 0.16		Gaussian *	DELPHI	this paper
$p/\overline{p}$	3.00 $\pm$ 0.09			OPAL	[9]
Λ^0	2.87 $\pm$ 0.13	0.18	distorted Gaussian *	ALEPH	[19]
Λ^0	2.79 $\pm$ 0.06		distorted Gaussian *	DELPHI	[14]
Λ^0	2.83 $\pm$ 0.13		limited spectrum	L3	[18]
Λ^0	2.77 $\pm$ 0.05		Gaussian	OPAL	[23]
Ξ^-	2.60 $\pm$ 0.16	0.16	Gaussian *	DELPHI	[16]
Ξ^-	2.57 $\pm$ 0.11		Gaussian	OPAL	[23]

Table 6: Position of the maximum in the ξ-distribution and their decay corrections ($\Delta\xi^*_{\rm decays}$) for different particles measured at LEP.

6 Summary and Conclusion

In the present paper the measurements of the Cherenkov angles in two radiator media (gas and liquid) were used for the identification of charged particles. The differential cross-sections for the production of $K^\pm$ and $p/\overline{p}$ were measured as a function of x_p ($x_p = P/P_{beam}$) in the kinematical regions:

$$\begin{array}{lll} K^\pm & 0.018 < x_p < 0.078 \quad \text{and} \quad 0.22 < x_p < 0.50 \\ p/\overline{p} & 0.031 < x_p < 0.11 \end{array}$$

The average $K^\pm$ and $p/\overline{p}$ multiplicities per hadronic event were determined to be: $N_K = 2.26 \pm 0.18$ and $N_p = 1.07 \pm 0.14$. Compared to the measurements, the JETSET model for the $K^\pm$ spectrum is a little softer at high momenta and the $p/\overline{p}$ rate is 10.5 % higher in the measured momentum region. The measured spectra are in agreement with measurements from OPAL [9] and ALEPH [20].

The differential cross-sections as a function of ξ ($\xi = \ln(1/x_p)$) are approximately Gaussian shaped. The maxima ξ^* of the measured distributions are: ${\xi^*}_K = 2.63 \pm 0.07$ and ${\xi^*}_p = 2.96 \pm 0.16$.

The measured ξ-distributions for various identified particles indicate a different mass dependence of ξ^* for mesons and baryons. The differences between mesons and baryons

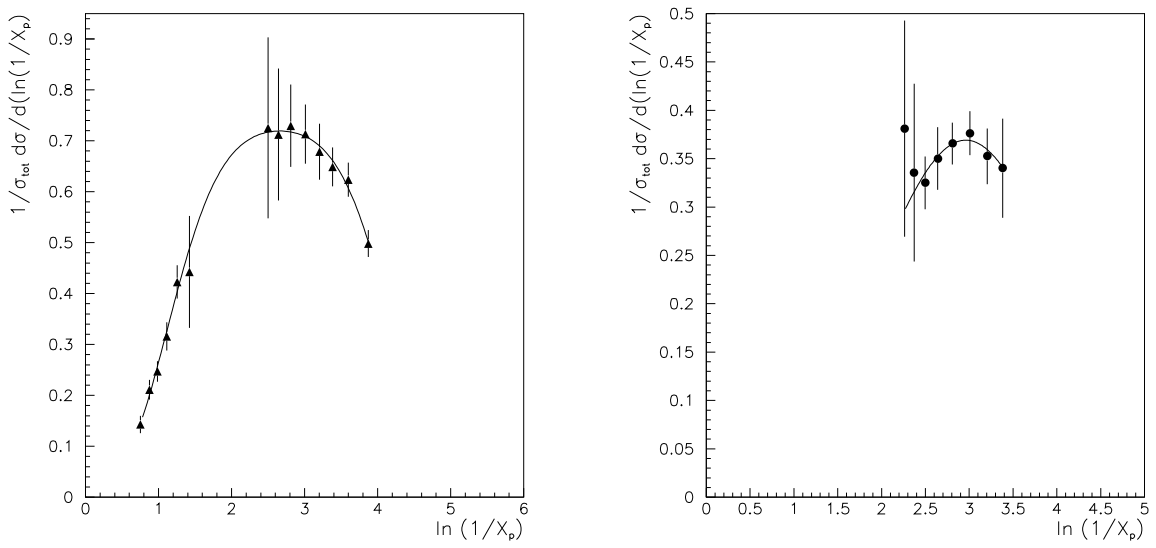

(a) $K^{\pm}$ (b) $p/\overline{p}$

Figure 8: Kaon and proton ξ distributions ($\xi = \ln(1/x_p)$). The full curves show the fit through the data.

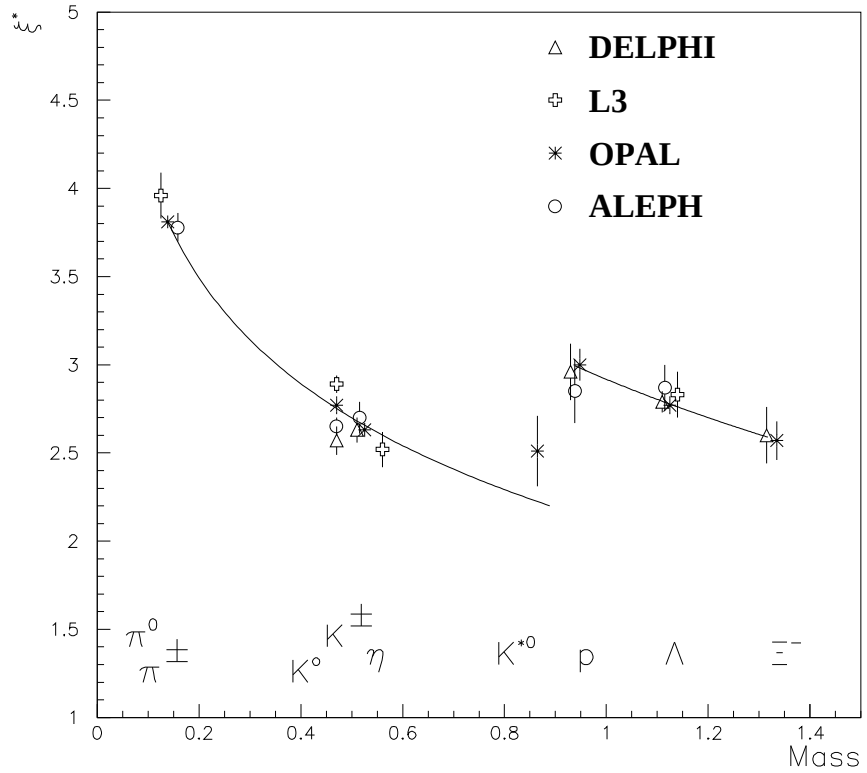

Figure 9: The maximum ξ^* of the ξ-distribution is shown as function of the particle mass. The full lines are separated fits for the meson and baryon distribution with $\xi^* \propto -\log(M_{hadron})$.

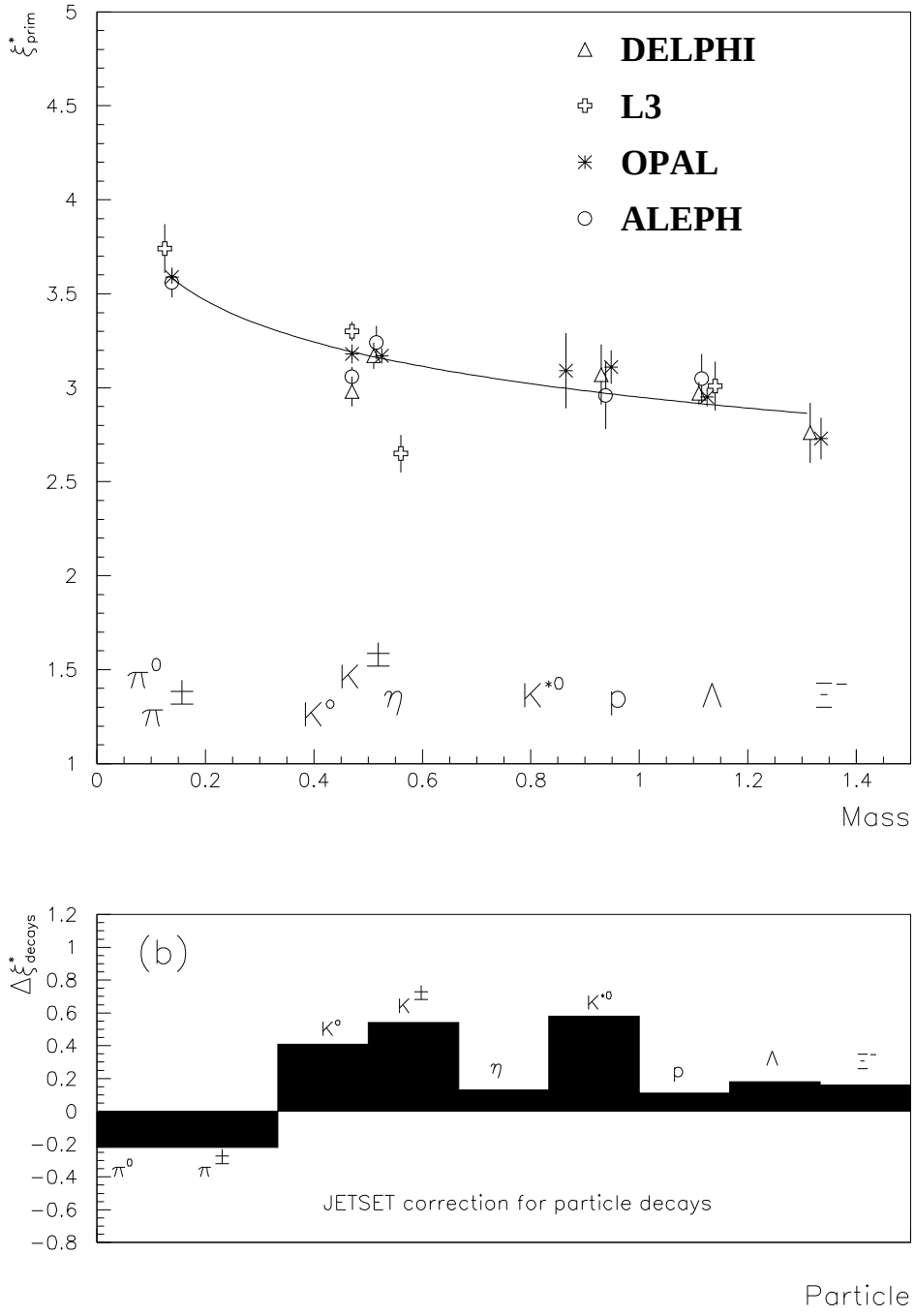

Figure 10: The maximum $\xi^*_{\rm prim}$ of the ξ distribution for primary hadrons is shown as function of the particle mass. The full line is a fit $\xi^*_{\rm prim} \propto -\log(M_{hadron})$ through the data points. The peak position is corrected for shifts coming from particle decays using the JETSET 7.3 model (1994 DELPHI tuning). The errors drawn do not include any contribution for the decay corrections. Figure (b) shows the size of the applied decay correction.

can be explained by shifts in the ξ^*-values due to particle decays which were extracted using the JETSET model. The observed mass dependence for the corrected $\xi^*_{\rm prim}$-values is in agreement with the prediction of the MLLA+LPHD model.

Acknowledgements

We are greatly indebted to our technical collaborators and to the funding agencies for their support in building and operating the DELPHI detector, and to the members of the CERN-SL Division for the excellent performance of the LEP collider.

References

[1] J.Drees, *Workshop on QCD, Aachen June 9-13 1992* Vol.1 page 106, and references quoted therein.

[2] Y.I. Azimov,Y.L.Dokshitzer,V.A.Khoze and S.I.Troyan, Z. Phys. C27 (1985) 65 and C31 (1986) 213.

[3] T. Sjöstrand, Comp. Phys. Comm. 39 (1986) 347;
T. Sjöstrand and M. Bengtsson, Comp. Phys. Comm. 43 (1987) 367;
T. Sjöstrand, CERN-TH 6488/92.

[4] G.Marchesini B.Webber, Nucl. Phys. B 310 (1988) 461;
G.Marchesini et al.,Comp. Phys. Comm. 67 (1992) 465.

[5] DELPHI collaboration, P. Abreu et al.: Nucl. Inst. Meth. A303 (1991) 233.

[6] E.G. Anassontzis et al., Nucl. Inst. Meth. A323 (1992) 351-362;
W. Adam et al., Nucl. Inst. Meth. A338 (1994) 284-309.

[7] T. Altherr and J. Seixas, Nucl. Inst. Meth. A317 (1992) 335-338.

[8] L. Lyons, *Statistics for nuclear and particle physicists*, Cambridge University Press 1986.

[9] OPAL collaboration, R. Akers et al.: Z. Phys. C 63 (1994) 181.

[10] DELSIM Users Guide, Internal Note DELPHI 87-86 PROG-99 (1989);
DELSIM Reference Manual Internal Note DELPHI 87-98 PROG-100 (1989).

[11] A.H. Mueller, in Proc. 1981 Intern. Symp. on Lepton and Photon Interactions at High Energies ed. W.Pfeil (Bonn 1981) 689;
Y.L. Dokshitzer, V.S.Fadin and V.A Khoze, Phys. Lett. B 115 (1982) 242.

[12] C.P. Fong and B.R. Webber, Phys. Lett. B 229 (1989) 289;
Y.L. Dokshitzer, V.A. Khoze and S.I. Troyan, Z. Phys. C 55 (1992) 107.

[13] DELPHI collaboration, P. Abreu et al.: Production characteristics of K^0 and light meson resonances in hadronic Z^0 decays CERN-PPE/94-130 subm. to Z. Phys. (1994).

[14] DELPHI collaboration, P. Abreu et al.: Phys. Lett. B 318 (1993) 249.

[15] Y.L.Dokshitzer,V.A.Khoze and S.I.Troyan Z. Phys. C 55 (1992) 107.

[16] DELPHI collaboration, P. Abreu et al.: contributed paper to the $27^{th.}$ International Conference on High Energy Physics in Glasgow ICHEP 94 Ref. gls0183 (1994).

[17] Y.L.Dokshitzer,V.A.Khoze and S.I.Troyan J. Phys. G 17 (1991) 1481.

[18] L3 collaboration, M. Acciarri et al.: Phys. Lett. B 328 (1994) 223.

[19] ALEPH collaboration, D. Buskulic et al.: Z. Phys. C 64 (1994) 361.

[20] ALEPH collaboration, D. Buskulic et al.: Inclusive $\pi^{\pm}$, $K^{\pm}$ and $(p,\overline{p})$ differential cross-sections at the Z resonance CERN-PPE/94-201 subm. to Z. Phys. (1994).

[21] OPAL collaboration, G. Alexander et al.: Phys. Lett. B 264 (1991) 467.

[22] OPAL collaboration, P.D. Acton et al.: Z. Phys. C56 (1992) 521.

[23] OPAL collaboration, P.D. Acton et al.: Phys. Lett. B 291 (1992) 503.